

# Improving performances of MCMC for Nearest Neighbor Gaussian Process models with full data augmentation

Sébastien Coube · Benoît Liqueur

Received: date / Accepted: date

**Abstract** Even though Nearest Neighbor Gaussian Processes (NNGP) alleviate considerably MCMC implementation of Bayesian space-time models, they do not solve the convergence problems caused by high model dimension. Frugal alternatives such as response or collapsed algorithms are an answer. Our approach is to keep full data augmentation but to try and make it more efficient. We present two strategies to do so.

The first scheme is to pay a particular attention to the seemingly trivial fixed effects of the model. We show empirically that re-centering the latent field on the intercept critically improves chain behavior. We extend this approach to other fixed effects that may interfere with a coherent spatial field. We propose a simple method that requires no tuning while remaining affordable thanks to NNGP's sparsity.

The second scheme accelerates the sampling of the random field using Chromatic samplers. This method makes long sequential simulation boil down to group-parallelized or group-vectorized sampling. The attractive possibility to parallelize NNGP likelihood can therefore be carried over to field sampling.

We present a R implementation of our methods for

---

Funding was provided by the Energy Environment Solutions (E2S-UPPA) consortium and the BIGCEES project from E2S-UPPA ("Big model and Big data in Computational Ecology and Environmental Sciences").

---

Sébastien Coube

Laboratoire de Mathématiques et de leurs Applications, Université de Pau et des Pays de l'Adour, UMR CNRS 5142, E2S-UPPA, Pau, France E-mail: sebastien.coube@univ-pau.fr

Benoît Liqueur

Laboratoire de Mathématiques et de leurs Applications, Université de Pau et des Pays de l'Adour, UMR CNRS 5142, E2S-UPPA, Pau, France  
Department of Mathematics and Statistics, Macquarie University, Sydney E-mail: benoit.liqueur@univ-pau.fr

Gaussian fields in the public repository

[https://github.com/SebastienCoube/Improving\\_NNGP\\_full\\_augmentation](https://github.com/SebastienCoube/Improving_NNGP_full_augmentation). An extensive vignette is provided.

We run our implementation on two synthetic toy examples along with the state of the art package `spNNGP`. Finally, we apply our method on a real data set of lead contamination in the United States of America mainland.

**Keywords** Nearest Neighbor Gaussian Process · Space-time models · Chromatic Sampler · Interweaving

## 1 Introduction

Many social or natural phenomena happen at the scale of a territory and must be observed at various sites and possibly times. The rise of modern GPS and Geographic Information Systems made large and high-quality point-referenced data sets more and more available. Let's assume that, in a collection of sites  $\mathcal{S}$  of the space or space-time domain  $\mathcal{D}$ , we have measurements  $z(\cdot)$  with some kind of space or space-time coherence. This coherence can be accounted for by introducing a spatially-indexed process  $w(\cdot)$  that has a well-defined joint distribution on any finite subset of the domain. We consider a Gaussian model where the observations  $z(\cdot)$  have been perturbed by a Gaussian noise  $\epsilon$  of standard deviation  $\tau$ . Many models also add linear regression on covariates  $X(\cdot)$ , giving the following classical model formulation

$$z(s) = X(s)\beta^T + w(s) + \epsilon(s), s \in \mathcal{S}.$$

Gaussian processes (GP) make an elegant prior distribution for  $w(\cdot)$  for continuous data (Gelfand et al. (2010)). The GP prior distribution of  $w(\mathcal{S})$  is  $\mathcal{N}(\mu, \Sigma)$ . The mean parameter of  $w(\cdot)$  is usually fixed to 0 to

avoid identification problems with the linear regression intercept  $\beta_0$ . The covariance matrix is usually computed using a positive definite function  $k(\cdot)$  with covariance parameters  $\theta$ , such as Matérn’s covariance and its exponential and squared-exponential special cases (Stein (1999); Joseph Guinness (2018)). It can then be written as  $\Sigma(\mathcal{S}, \theta)$ , and its entries are  $\Sigma(\mathcal{S}, \theta)_{i,j} = k(s_i, s_j, \theta)$ . The covariance parameters can have modeller-specified hyperpriors (Fuglstad et al. (2015); Datta et al. (2016)). The weakness of Gaussian processes is that computing the GP prior density of  $w(\mathcal{S})$  involves the determinant and inverse of  $\Sigma(\mathcal{S}, \theta)$ , incurring a computational cost that is cubic in the size of  $\mathcal{S}$ . Vecchia’s approximation to Gaussian likelihoods received increased attention the past years, with theoretical developments (Katzfuss and Guinness (2017); Guinness (2018); Datta et al. (2016); Finley et al. (2019)) and software (Joseph Guinness (2018); Finley et al. (2017)). Nearest Neighbor Gaussian Process (NNGP) is a special case of Vecchia’s approximation that allows to find a surrogate of the the inverse Cholesky factor of  $\Sigma$  and use it to approximate GP prior density. It starts by finding an ordering for the  $n$  locations of  $\mathcal{S}$  which we will note  $(s_1, \dots, s_n)$ . The ordering may have an impact on the quality of the approximation, and is discussed by Datta et al. (2016); Guinness (2018).

The joint latent density of  $w(s_1, \dots, s_n)$  is then written under the recursive conditional form :

$$f(w(s_1, \dots, s_n) | \theta, \mu) = f(w(s_1) | \theta, \mu) \times \prod_{i=2}^n f(w(s_i) | w(s_1, \dots, s_{i-1}), \theta, \mu).$$

Since  $f(w(s_1, \dots, s_n) | \theta, \mu)$  is a Multi-Variate Normal (MVN) distribution function, the conditional density  $f(w(s_i) | w(s_1, \dots, s_{i-1}), \theta, \mu)$ ,  $i \in 2, \dots, n$  is a Normal as well.

Nearest Neighbor Gaussian Process consists, for each conditional density, in replacing the vector  $w(s_1, \dots, s_{i-1})$  that conditions  $w(s_i)$  by a much smaller parent subset noted  $w(pa(s_i))$ . NNGP approximation to the GP prior joint density of  $w(\cdot)$  is defined as

$$\tilde{f}(w(s_1, \dots, s_n) | \theta, \mu) = f(w(s_1) | \theta, \mu) \times \prod_{i=2}^n f(w(s_i) | w(pa(s_i)), \theta, \mu). \quad (1)$$

This very general principle can be applied to any kind of well-defined multivariate density. However, as far as we know, MVN density approximation is the only application. This may be explained by the fact that non-Gaussian data can be handled with GP modelling thanks to link functions. Moreover, NNGP defines a MVN density and allows to compute explicitly and easily the sparse Cholesky factor of the precision matrix.

The choice of the parents is critical but no universal criterion exists. A popular choice is to choose the parent locations  $pa(s_i)$  as  $s_i$ ’s nearest neighbors among  $(s_1, \dots, s_{i-1})$ , explaining the denomination “Nearest Neighbors Gaussian Process” given by Datta et al. (2016). Other schemes exist like mixing close and far-away observations (Datta et al. (2016); Stein et al. (2004)). This approximation is cheap and easily parallelisable. The latent density (1) can be split into small jobs and dispatched to a cluster of calculators (Datta et al. (2016)). Its cost is linear in the number of observations under the condition that the size of each parent set is bounded. More advanced strategies exist such as grouping, proposed by Guinness (2018).

If NNGP allows to work around the bottleneck of GP likelihood computation, it does not solve the problem of slow MCMC convergence. In Datta et al. (2016), the Gibbs sampler loops over  $\theta$ ,  $w(\mathcal{S})$  and  $\beta$ ,  $\mu$  is fixed to 0. The latent field  $w(\mathcal{S})$  is updated sequentially or by blocks. This sampler suffers from slow mixing, in particular when  $n$  increases. Other strategies have been proposed by Finley et al. (2019) that precisely avoid to sample the field in order to reduce the dimension of the model.

Our approach is nevertheless to improve NNGP implementations where the latent field is explicitly sampled. Our first reason is that there may be situations where some of the methods presented in Finley et al. (2019) perform poorly while full data augmentation works well. For example, the *collapsed NNGP* (Finley et al. (2019)) enjoys low dimensionality and allows nonetheless to retrieve the latent field, but demands Cholesky factorization of large sparse matrices which may be unfeasible depending on  $n$  and the dimension of  $\mathcal{D}$  (Finley et al. (2019); Rue and Held (2005)). The *Response NNGP* (Finley et al. (2019)) allows to retrieve the covariance parameters  $\theta$  but not the latent field  $w(\mathcal{S})$ .

Our second reason is that efficient Gibbs sampler architectures can sharply improve mixing. NNGP defines a Markov Random Field, allowing to use the blocking methods of Knorr-Held and Rue (2002). The sparse Cholesky factor in NNGP allows to use the Ancillary-Sufficient Interweaving Strategy (ASIS) presented by Yu and Meng (2011). The third reason is that full latent field sampling is all terrain, and can address many data models or be plugged into complex, non-stationary models (Heinonen et al. (2016)).

Here is an outline of the article. Section 2 focuses on the seemingly trivial fixed effects of the hierarchical model. In 2.1 we propose a mild but efficient centering of the latent field on the least squares regression intercept. In 2.2, we extend centering to other fixed effects,

and we use interweaving (Yu and Meng (2011)) to propose a robust, tuning-less application. Section 3 targets the simulation of the random field. In 3.1, we propose to use the chromatic samplers developed by Gonzalez et al. (2011) in order to carry the attractive parallelizability of Vecchia likelihood over to field sampling. In 3.2, we analyze the sensitivity of NNGP graph coloring and we benchmark coloring algorithms. We apply our methods in section 4. We present our implementation (available at [https://github.com/SebastienCoube/Improving\\_NNGP\\_full\\_augmentation](https://github.com/SebastienCoube/Improving_NNGP_full_augmentation)) in 4.1. We test our implementation along with the state of the art package spNNGP (Finley et al. (2017)) on synthetic toy examples in 4.2. In 4.3, we present an application on lead contamination in the mainland of the United States of America. The article ends by a discussion in Section 5.

## 2 Latent field centering

### 2.1 Centering the latent field on the intercept

The mean parameter  $\mu$  of the prior density for the latent field  $w(\cdot)$  is usually set to 0 in order avoid identification problems with the intercept  $\beta_0$ . We call this formulation standard, since it is found in state of the art papers such as Datta et al. (2016); Finley et al. (2019). We name samples of the standard formulation  $w_s(\cdot)$ . Our proposal is to replace  $w_s(\mathcal{S})$  by a centered  $w_c(\mathcal{S}) = w_s(\mathcal{S}) + \beta_0$  in the Gibbs Sampler. This substitution is a non degenerate linear transform that keeps the model valid and allows to retrieve samples from standard parametrization if needed.

The centered parametrization can also be seen as a slightly different model that changes the prior density of the latent field and the likelihood of the observed field. The NNGP prior goes from  $\tilde{f}(w_s(\mathcal{S})|0, \Sigma(\mathcal{S}, \theta))$  to  $\tilde{f}(w_c(\mathcal{S})|\beta_0, \Sigma(\theta))$ . On the other hand, the likelihood's mean parameter goes from  $w_s(\mathcal{S}) + \beta_0 + X(\mathcal{S})\beta^T$  to  $w_c(\mathcal{S}) + X(\mathcal{S})\beta^T$ .

Those changes impact the full conditional distributions. We give a table (1) that summarizes the changes in a Gibbs sampler for a Gaussian model that loops over the parameters (Datta et al. (2016)). We note  $\phi(\cdot|\cdot, \cdot)$  the normal density function, and  $\tilde{Q}$  the latent field's precision matrix defined by NNGP. We abbreviate the interest variables  $X(\mathcal{S})$  as  $X$ . We note the vector made of  $n$  times 1 as  $\mathbf{1}$ . The matrix obtained by adding  $\mathbf{1}$  to the left side of  $X$  is named  $[\mathbf{1}|X]$ . We did not feature prior distributions on the high-level parameters like  $\theta$ ,  $\tau$  or  $\beta$ : their full conditionals would not be affected since centering changes only the NNGP prior and the observed data likelihood. Even if the modification is minor, the improvement in the mixing of the intercept is clear. We

simulated a little toy example with 1000 observations and we ran the two Gibbs sampler. The autocorrelation plots (Figure 1) are clearly in favor of the centered formulation. Even though for this toy example the standard model mixes after a few hundred iterations, this is not the case for larger cases. We strongly suspect that R package spNNGP (Finley et al. (2017)) also uses the centered model, even though the reference of the package is Datta et al. (2016) which uses the standard model.

We observed empirically that there is much more correlation between  $w(\mathcal{S})$  and  $\beta_0$  in the standard implementation. Plotting  $\frac{1}{n}\Sigma w(\mathcal{S})$  against  $\beta_0$  (Figure 2) allows to see a clear ridge in the case of the standard model (Figure 2b). This means that the whole latent field has to shift upwards and downwards for the intercept to explore its posterior distribution, causing a slow exploration.

Ridge-like densities are a well known plague of Gibbs samplers, and linear recombination is one of the tools that allows to get rid of it (Gelfand et al. (1995)).

In the next sections, we use the centered model and we note the latent field  $w(\cdot)$ .

### 2.2 Extension to other fixed effects

Field centering can be extended to other fixed effects. In most cases it is unnecessary because centering and scaling  $X(\mathcal{S})$  is enough to considerably improve chain behavior. Even worse, the Gibbs sampler usually behaves very bad if the random field is centered on other fixed effects than the intercept. There are nonetheless cases where bad mixing of the regression coefficients happens again. In this case, it is often useful to try and center  $w(\cdot)$  not only on the intercept but also on the troublesome covariates' fixed effect. However, doing preliminary runs and picking manually which fixed effects the field needs to be centered on would be tedious. Interweaving (Yu and Meng (2011)) allows to combine very simply the advantages of the two strategies and removes the need to choose.

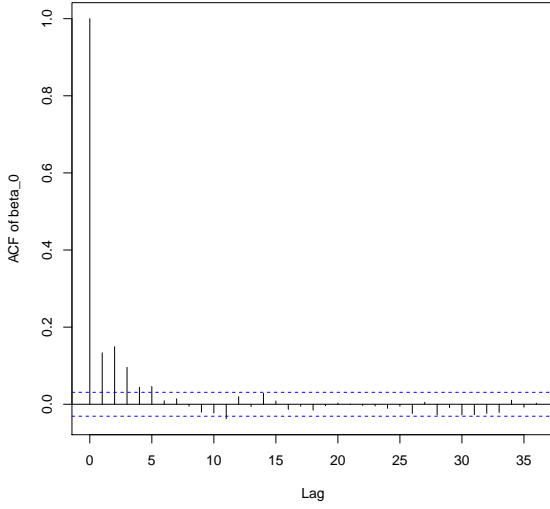
There are two limitations to this approach. The first is the case where several measurements of the interest variable  $z(\cdot)$  and the regressors  $X(\cdot)$  are done at the same spatial location. The model must be extended as

$$z(s, i) = X(s, i)\beta^T + w(s) + \epsilon(s, i), s \in \mathcal{S}, 1 \leq i \leq m(s),$$

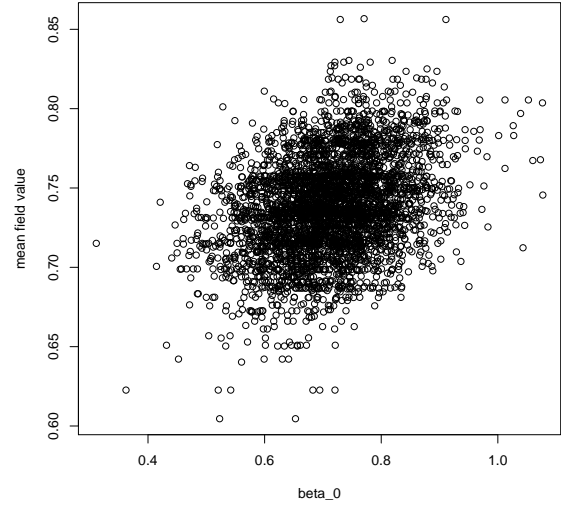
$m(s) \geq 1$  being the number of observations in the site  $s$ . In this setting, some variables vary within one spatial locations while other do not. For example, the presence of asbestos in buildings may be considered as a location-wise regressor while smoking is an observation-wise regressor. If the regressors vary within one location, it

Table 1: Changes in the full conditional distributions

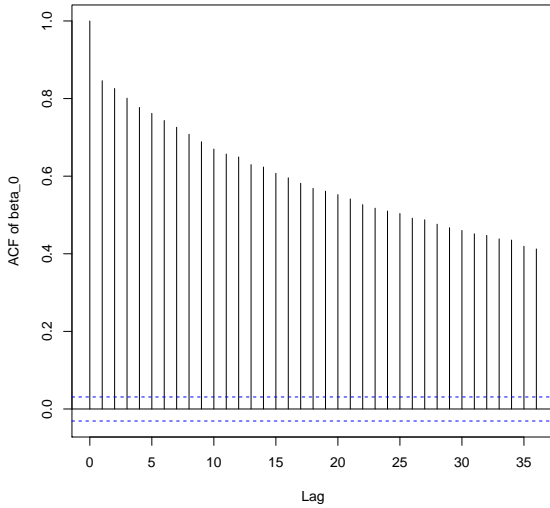
Variable	Standard	Centered
$\beta_0$		$\phi(\beta_0, (\mathbf{1}^T \mathbf{Q} \mathbf{1})^{-1} (\mathbf{1}^T \mathbf{Q} w_c), (\mathbf{1}^T \mathbf{Q} \mathbf{1})^{-1})$
$\beta$		$\phi(\beta, (X^T X)^{-1} (X^T z(\mathcal{S})), \tau^2 (X^T X)^{-1})$
$(\beta_0, \beta)$	$\phi(\beta, ([\mathbf{1} X]^T [\mathbf{1} X])^{-1} ([\mathbf{1} X]^T z(\mathcal{S})), \tau^2 ([\mathbf{1} X]^T [\mathbf{1} X])^{-1})$	
$\theta$	$\tilde{f}(w_s(\mathcal{S}) 0, \theta)$	$\tilde{f}(w_c(\mathcal{S}) \beta_0, \theta)$
$\tau$	$\prod_{s \in \mathcal{S}} \phi(z(s) w_s(s) + \beta_0 + X(s)\beta^T, \tau)$	$\prod_{s \in \mathcal{S}} \phi(z(s) w_c(s) + X\beta^T, \tau)$
$w(x), x \in \mathcal{S}$	$\tilde{f}(w_s(x) w_s(\mathcal{S} \setminus x), 0, \theta)$ $\phi(z(x) w_s(x) + \beta_0 + X(x)\beta^T, \tau)$	$\tilde{f}(w_c(x) w_c(\mathcal{S} \setminus x), \beta_0, \theta)$ $\phi(z(x) w_c(x) + X(x)\beta^T, \tau)$



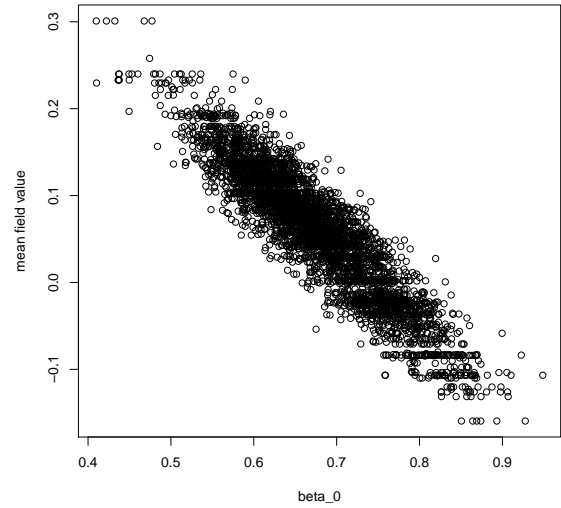
(a) Centered model



(a) Centered model



(b) Standard model



(b) Standard model

Fig. 1: The ACF of  $\beta_0$  drops much faster in the centered model than in the standard modelFig. 2: When plotting  $\frac{1}{n} \Sigma w(\mathcal{S})$  against  $\beta_0$ , the standard model exhibits a ridge-shaped point cloud

is impossible to center the field on the corresponding fixed effects. This would mean that the normal random variable  $w(s)$  has several mean parameters at the same time. However, it is still possible to restrict interweaving to the regression coefficients associated to the location-wise variables. Our implementation allows to specify which regressors are associated to spatial location and which are associated to individual measurements.

NNGP being a point-measurement model, regressors obtained through gridded and areal data are immediately eligible for this method. The second limitation is the computational cost. With improper constant prior, the centered regression coefficients follow a MVN distribution with mean  $(X^T \tilde{Q}(\theta) X)^{-1} (X^T \tilde{Q}(\theta) (w_c + X \beta^T))$  and covariance  $(X^T \tilde{Q}(\theta) X)^{-1}$ . The parameters need to be computed at each update of  $\theta$ . The sparsity induced by Vecchia approximation is critical for the feasibility of the method because it ensures that matrix multiplications involving  $\tilde{Q}$  are affordable. Using sparse matrix formulation for  $X$  could further alleviate this operation if  $X$  has dummy variables or null measurements.

We present the steps to update the regression coefficients with interweaving. The notations are the same as in subsection 2.1. For the sake of simplicity, we suppose that there is only one measurement of  $X$  per spatial location and we use an improper constant joint hyperprior on  $(\beta_0, \beta)$ . The parameters that depend on the state in the Gibbs sampler are indexed by  $t$ . When some variables from  $X$  are not suitable for interweaving, the corresponding components of  $\beta$  do not undergo step 4. It is also necessary to match the observations and the spatial locations to apply interweaving. If the observations were not Gaussian, this step would be left unchanged while step 2 would be adapted just like in any generalized NNGP model (Datta et al. (2016)).

### 3 Chromatic sampler for Nearest Neighbor Gaussian Process

#### 3.1 Chromatic samplers and how to apply them to NNGP

If conditionally independent variables follow each other in a Gibbs sampler, then they can be updated in parallel. Let's consider a Gibbs sampler or a Metropolis-Within-Gibbs aiming to sample from a joint multivariate

distribution  $f(x_1, \dots, x_n)$ .

$$\begin{aligned} x_1^{t+1} &\sim f(x_1 | x_2^t, \dots, x_n^t) \\ &\dots \\ x_i^{t+1} &\sim f(x_i | x_1^{t+1}, \dots, x_{i-1}^{t+1}, x_{i+1}^t, \dots, x_n^t) \\ &\dots \\ x_n^{t+1} &\sim f(x_n | x_1^{t+1}, \dots, x_{n-1}^{t+1}). \end{aligned}$$

Let's introduce  $p \leq n$  vectors  $X_1, \dots, X_p$  so that  $(x_1, \dots, x_n) = (X_1, \dots, X_p)$ , and suppose that  $\forall X \in X_1, \dots, X_p$ , either  $X$  has only one element or the elements of  $X$  are conditionally independent given the other variables. The Gibbs sampler can then be re-written

$$\begin{aligned} x_i^{t+1} \in X_1 &\sim f(x_i | X_2^t, \dots, X_p^t) \\ &\dots \\ x_i^{t+1} \in X_j &\sim f(x_i | X_1^{t+1}, \dots, X_{j-1}^{t+1}, X_{j+1}^t, \dots, X_p^t) \\ &\dots \\ x_i^{t+1} \in X_p &\sim f(x_i | X_1^{t+1}, \dots, X_{p-1}^{t+1}). \end{aligned}$$

Since all elements from  $X_j$  are simulated from independent densities, it is possible to parallelize their sampling.

The chromatic samplers developed in Gonzalez et al. (2011) use graph coloration algorithms to find groups of conditionally independent variables that allow block-parallel Gibbs sampling on a Gaussian Markov Random Field (GMRF). A useful point is that chromatic samplers can be applied to block sampling as well. Let  $A$  be the  $n_1 \times n_1$  adjacency matrix of a GMRF and let  $B$  be a  $n_1 \times n_2$  matrix,  $n_1$  being her the number of variables of the GMRF and  $n_2$  the number of blocks.  $B_{i,j} = 1$  if variable  $i$  belongs to block  $j$ , and 0 otherwise. Then,  $B^T A B$  indicates the connections between the blocks and the graph it defines can be used for chromatic block sampling.

Using inductively the Global Markov property, it is possible to guarantee mutual conditional independence for the variables or the blocks that correspond to vertices sharing the same color. NNGP is defined on a Directed Acyclic Graph (DAG) (Datta et al. (2016); Katzfuss and Guinness (2017)). Then, using the argument of recursive kernel factorization given by Lauritzen (1996), it has the Markov properties on the moral graph obtained by un-directing the edges and "marrying" the parents in the DAG (Figure 3). Chromatic sampling can be applied straightforwardly to Datta et al. (2016). It also allows to compute normalizing constants and can be combined with the covariance parameter blocking proposed by Knorr-Held and Rue (2002).



**Algorithm 1** Regression coefficient updating with interweaving

---

```

1: input  $\tilde{Q}^t, w^t, X, \beta^t, \beta_0^t, \tau^t$ 
2: simulate  $\beta^{t+.5}$  with density  $\phi(\beta, (X^T X)^{-1}(X^T z), \tau^2(X^T X)^{-1})$ 
3:  $v = w^t + X(\beta^{t+.5})^T$ 
4: simulate  $\beta_0^{t+1} \beta^{t+1}$  with density  $\phi(\beta_0, ([\mathbf{1}|X]^T \tilde{Q}^t [\mathbf{1}|X])^{-1}([\mathbf{1}|X]^T \tilde{Q}^t v), ([\mathbf{1}|X]^T \tilde{Q}^t [\mathbf{1}|X])^{-1})$ 
5: return  $\beta_0^{t+1} \beta^{t+1}$ 

```

---

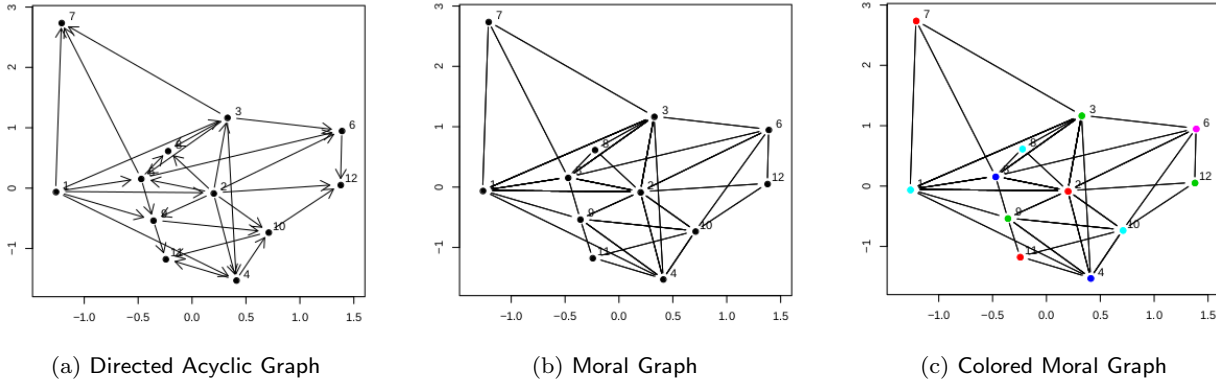


Fig. 3: Moralization and coloring of a DAG

### 3.2 Coloring of NNGP moral graphs : sensitivity analysis and algorithms benchmark

Coloring the moral graph  $\mathcal{G}^m$  is a critical step in chromatic sampling and determines the attractiveness of the method with respect to the “vanilla” versions of the algorithms (one-site sequential sampling or blocked sampling with several blocks). We focus on two variables to summarize the efficiency of chromatic sampling :

- The number of colors : the smaller this number, the fewer the number of steps in the chromatic sampler.
- The time needed for coloring, that must be small with respect to the running time of the MCMC chains

This section has two objectives. The first is to test the sensitivity of those two interest variables to the properties of  $\mathcal{G}^m$  and the coloring algorithm using variance-based sensitivity analysis. The second objective is to benchmark various coloring algorithms and find a rule to choose the algorithm.

We test various factors that may change the structure of  $\mathcal{G}^m$  :

- Size  $n$
- Number of parents in the DAG  $m$
- Spatial domain dimension  $d$
- Ordering of the points

We also test 3 coloring algorithms :

- Naive greedy coloring : coloring each vertex with the smallest available color.

- Degree greedy coloring : reorder the vertices following their number of neighbors, and apply naive greedy coloring.
- DSATUR heuristic : color the node that has the highest number of distinct colors among its neighbors, and break ties using the number of neighbors.

#### 3.2.1 Pilot experiment

##### Design

The objective is to do preliminary sensitivity analysis and benchmark on small graphs. We test for the three coloring algorithms and for graphs with the following attributes :

- Graph size  $n = 500, 1000, 2000$ .
- Number of parents  $m = 5, 10, 20$ .
- Dimension  $d = 2, 3$ .
- Ordering following the first coordinate (Datta et al. (2016)), at random, or using MaxMin heuristic (Guinness (2018)).

Each case is replicated 10 times.

##### Sensitivity

The color count is overwhelmingly driven by the number of parents, the ordering, and interactions between them. It is robust with respect to the graph size because  $n$  and its interactions have very low percentages in table 2. Since the numbers of colors are small with respect to  $n$  (45 colors at the most), this makes chromatic sampling a good candidate for large data sets. Surprisingly

enough, the dimension of the points  $d$  plays almost no role. The choice of the coloring algorithm has a very marginal effect on the color count.

The running time is affected by  $n$ , as expected. However, it is mostly explained by the coloring algorithm and its interactions with  $n$  and  $m$ .

This sensitivity analysis is best complemented with a visual exploration. In Figure 4, we see the results of the experiment when the ordering of the spatial points is random and  $d = 2$ . The number of parents  $m$  defines well-separated vertical clouds of points, showing a clear, positive impact on the number of colors. It also increases the running time : the clouds of points on the right are stretched higher along the ordinates axis. The graph size  $n$  affects positively the running time. The other cases with different ordering and dimension all show this clear, chromatography-like profile.

Table 2: Sensitivity analysis

Read : “In the pilot experiment, the ordering of the spatial points explained 15.4 percents of the variance of the number of colors”

	Pilot		Large		Blocked	
	colors	time	colors	time	colors	time
ordering	15.4	3.4	10.6	8.7	40.7	1.7
algo	0.8	24.7	0.5	1.3	1.0	8.6
d	0.6	0.0	1.1	0.7	0.0	0.0
m	76.4	2.8	80.6	26.0	4.9	0.4
n/n blocks	0.2	11.8	0.1	40.7	8.9	6.4
ordering:algo	0.3	6.8	0.1	0.3	0.3	3.3
ordering:d	0.3	0.0	0.5	0.4	0.0	0.0
ordering:m	5.3	0.8	5.2	5.4	2.3	0.2
ordering:n	0.0	3.3	0.0	3.0	4.1	2.5
algo:d	0.0	0.1	0.0	0.0	0.0	0.0
algo:m	0.2	5.5	0.2	0.6	0.0	0.9
algo:n	0.0	23.3	0.0	0.7	0.4	12.4
d:m	0.2	0.0	0.4	0.5	12.3	0.6
d:n	0.0	0.0	0.0	0.2	1.5	1.5
m:n	0.0	2.4	0.0	8.0	7.3	8.9
total	99.7	84.8	99.5	96.6	83.7	47.6

### Benchmark

In order to see if one coloring algorithm has the better of the others, we compare the average number of colors for each case of the experiment in table 3. Regardless of the ordering,  $m$ , and  $n$ , the number of colors favors systematically but slightly DSATUR over the two simpler algorithms. In the case of coordinate ordering, naive greedy coloring reaches the performances of DSATUR. While the two simple methods are very economical, the running time becomes high in DSATUR when the graph size augments (Figure 4b).

We conclude that regardless of the structure of the graph, DSATUR must be chosen for smaller graphs. The two other methods must be chosen for larger graphs

because DSATUR will become prohibitively expensive.

### 3.2.2 Coloring for large graphs

#### Design

The objective is to test the sensitivity of the two interest variables and to benchmark coloring algorithms when the graphs are bigger. The experiment is the same as before, with two differences :

- Only naive greedy and degree greedy coloring algorithms are tested
- The graph size  $n = 50000, 100000, 200000$

Each case is replicated 10 times.

#### Sensitivity

For the number of colors, the results are the same as before (table 2). It is mostly determined by the ordering and the number of parents. The robustness of the number of colors with respect to  $n$  is confirmed.

The running time is affected mostly by  $n$ , but the ordering and  $m$  also play a role.

In table 4, we can see that naive coloring systematically has a lower mean number of colors than degree coloring. It is also slightly faster due to the fact that the vertices are not sorted. Anyway, the running times are short in both cases and are never bigger than 15 seconds. We conclude that naive greedy coloring is the better option for large data sets.

### 3.2.3 Coloring blocked graphs

#### Design

The objective is to carry out sensitivity analysis and benchmark to graphs that correspond to spatial blocks used for block-update of the latent field (Datta et al. (2016); Knorr-Held and Rue (2002)). Spatial clusters of vertices are found using a K-means algorithm on  $n = 10000$  spatial locations, and coloring is applied to the Markov graph between the blocks. The orderings, the numbers of parents, and the dimensions remain the same as in the previous experiments. The parameters that change are :

- The graph size  $n_{blocks} = 10, 20, 50, 100, 500$ .
- All three algorithms (DSATUR, naive greedy, and degree greedy) are tested

Each case is replicated 10 times.

#### Sensitivity

The sensitivity of the number of colors (table 2) differs from the previous experiments. Even though  $m$  remains important, it is the ordering that becomes the most important variable. The graph size also plays a bigger role

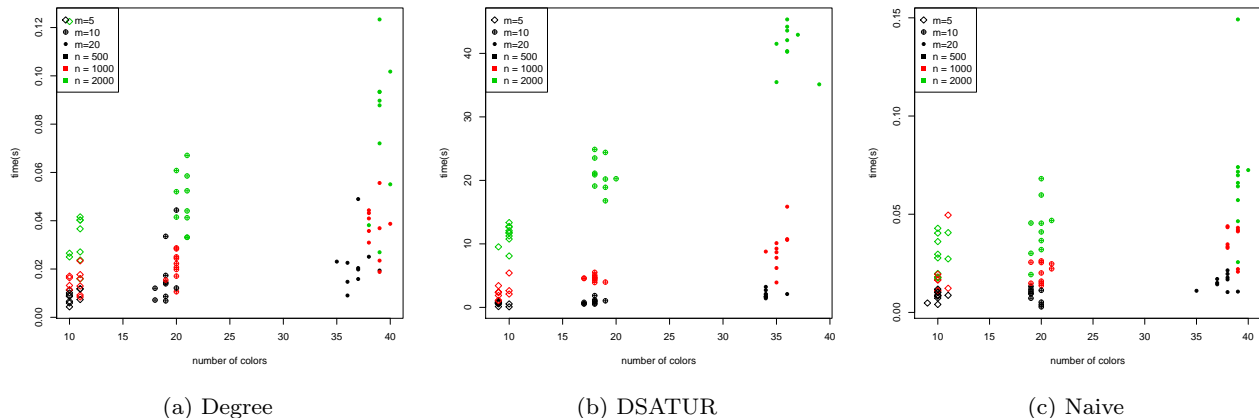


Fig. 4: Repartition of the number of colors and running time with random ordering and  $d=2$ .

Table 3: Case-by-case mean number of colors in the pilot experiment.

m	n	d	Coordinate ordering			Max-min ordering			Random ordering		
			degree	dsatur	naive	degree	dsatur	naive	degree	dsatur	naive
5	500	2	7.4	6.0	6.0	9.8	9.1	10.1	10.3	9.2	10.0
		3	7.9	6.0	6.0	10.8	9.6	11.0	10.6	10.0	11.1
	1000	2	8.2	6.0	6.0	10.1	9.4	10.3	10.6	9.3	10.2
		3	8.0	6.0	6.0	11.8	10.0	11.1	11.3	10.1	11.1
	2000	2	8.6	6.0	6.0	10.5	9.6	10.3	10.7	9.9	10.2
		3	8.9	6.0	6.0	11.6	10.1	11.7	11.8	10.0	11.4
10	500	2	12.9	11.0	11.0	18.7	17.4	18.9	19.0	17.8	19.4
		3	13.0	11.0	11.0	20.9	19.1	21.2	21.0	18.9	21.3
	1000	2	13.7	11.0	11.0	19.2	17.8	19.5	19.9	17.9	20.0
		3	13.6	11.0	11.0	21.3	19.4	22.3	21.6	19.4	22.0
	2000	2	14.8	11.0	11.0	20.2	18.2	20.0	20.7	18.6	19.8
		3	15.0	11.0	11.0	22.3	19.7	22.6	22.7	19.9	22.4
20	500	2	23.0	21.0	21.0	36.5	33.9	37.4	36.8	34.2	37.5
		3	23.3	21.0	21.0	40.8	37.1	44.1	40.5	37.5	43.4
	1000	2	24.9	21.0	21.0	37.6	35.0	38.2	38.6	35.2	38.5
		3	23.9	21.0	21.0	42.9	38.4	45.3	43.1	38.8	44.7
	2000	2	26.0	21.0	21.0	38.6	35.9	38.8	39.1	36.2	39.1
		3	25.7	21.0	21.0	44.8	39.6	46.4	44.7	40.0	45.6

as well. Case-by-case examination of the mean number of colors (table 5) allows to see that the coloring changes sharply with the ordering. Coordinate ordering always has low numbers of colors whatever  $m$  and  $n$ , while the other orderings have higher numbers of colors and are more sensitive to  $m$  and  $n$ .

#### Benchmark

Uncontestably, DSATUR has the smallest number of colors. Interestingly, degree greedy coloring has the second smallest number of colors. If we assume that the number of blocks will always be smaller than 1000, we can discard the running time from our criteria and say that DSATUR is the best option for blocked graphs. However, in the cases with random and Max-Min orderings and low numbers of blocks, chromatic sampling does not greatly reduce the number of steps with respect to vanilla block sampling.

## 4 Implementation, testing and application

### 4.1 About our implementation

We tested our implementation along with the state of the art package `spNNGP` Finley et al. (2017), that uses the NNGP Gibbs sampler architecture given by Datta et al. (2016). `spNNGP` uses `Rcpp` (Eddelbuettel et al. (2011)) and parallelizes the computation of NNGP likelihood. In order to monitor convergence using Gelman-Rubin-Brooks diagnostics (Gelman and Rubin (1992); Brooks and Gelman (1998)), various chains need to be run one after the other.

Our implementation is available at [https://github.com/SebastienCoube/Improving\\_NNGP\\_full\\_augmentation](https://github.com/SebastienCoube/Improving_NNGP_full_augmentation). The code is done in R (R Core Team (2018a)), with the ASIS Gibbs sampler architecture (Yu and Meng



Table 4: Case-by-case mean number of colors for large graphs.

m	n	d	Coordinate ordering		Max-min ordering		Random ordering	
			degree	naive	degree	naive	degree	naive
5	50000	2	10.0	8.8	11.3	11.0	12.3	11.1
		3	10.0	8.7	13.1	12.6	13.1	12.3
	100000	2	10.1	9.0	11.7	11.0	12.1	11.0
		3	10.0	9.1	13.1	13.0	13.2	12.3
	200000	2	10.1	9.3	11.9	11.2	12.1	11.4
		3	10.3	9.7	13.3	13.0	13.5	12.8
10	50000	2	17.1	13.8	21.5	21.0	22.7	20.8
		3	17.0	14.0	24.5	24.1	25.5	23.7
	100000	2	17.0	15.6	22.0	21.2	22.9	21.0
		3	17.0	15.5	24.9	24.2	25.6	23.9
	200000	2	17.9	16.7	22.2	21.3	22.9	21.1
		3	18.0	16.8	25.2	24.2	26.4	24.3
20	50000	2	31.4	21.1	41.4	40.1	43.0	40.4
		3	31.2	21.6	49.7	48.2	50.2	47.8
	100000	2	30.8	25.1	41.9	40.7	44.3	40.8
		3	31.0	24.6	50.0	48.5	50.8	47.6
	200000	2	30.3	28.6	41.7	40.7	44.3	40.8
		3	30.2	28.7	50.5	48.9	51.6	48.2

Table 5: Case-by-case mean number of colors for blocked graphs.

m	blocks	d	Coordinate ordering			Max-min ordering			Random ordering			
			degree	dsatur	naive	degree	dsatur	naive	degree	dsatur	naive	
5	10	2	2.9	2.5	3.0	6.2	6.2	6.6	6.5	6.5	6.7	
		3	2.7	2.3	2.7	7.5	7.5	7.5	7.3	7.3	7.5	
	20	2	3.0	2.4	3.0	7.9	7.9	8.6	7.6	7.5	8.3	
		3	3.0	2.6	3.0	9.0	8.5	9.6	8.6	8.3	9.5	
	50	2	3.0	2.4	3.0	8.9	8.6	10.8	8.6	8.1	10.2	
		3	3.0	2.4	3.0	10.9	10.2	12.7	10.3	9.4	12.0	
	100	2	3.0	2.4	3.0	9.8	9.1	12.0	9.0	8.6	11.3	
		3	3.0	2.2	3.0	11.8	11.1	14.0	11.0	10.2	13.0	
	500	2	3.0	2.9	3.1	10.3	9.3	14.7	10.1	9.1	14.3	
		3	3.0	3.0	3.0	13.2	11.7	17.3	12.4	11.1	16.1	
	10	10	2	2.9	2.5	3.0	8.1	8.1	8.2	8.6	8.6	8.6
			3	2.7	2.3	2.7	9.3	9.3	9.3	9.3	9.3	9.3
20		2	3.0	2.4	3.0	11.4	11.4	12.2	11.9	11.9	12.5	
		3	3.0	2.6	3.0	13.5	13.4	13.8	12.5	12.3	13.0	
50		2	3.0	2.4	3.0	14.8	14.2	17.1	14.0	13.6	16.0	
		3	3.0	2.4	3.0	17.5	16.6	19.0	16.2	15.5	18.2	
100		2	3.0	2.4	3.0	16.7	16.0	20.6	15.7	15.0	19.2	
		3	3.0	2.2	3.0	19.8	18.5	22.9	18.0	17.1	21.2	
500		2	3.6	3.1	4.1	19.6	18.2	26.5	18.6	17.0	24.5	
		3	3.8	3.4	4.3	22.9	21.0	30.9	20.9	18.8	28.0	
20		10	2	2.9	2.5	3.0	9.8	9.8	9.8	9.9	9.9	9.9
			3	2.7	2.3	2.7	10.0	10.0	10.0	10.0	10.0	10.0
	20	2	3.0	2.4	3.0	16.2	16.2	16.7	16.3	16.3	16.5	
		3	3.0	2.6	3.0	17.7	17.7	17.7	17.1	17.1	17.2	
	50	2	3.0	2.4	3.0	25.1	24.5	27.0	23.0	22.9	25.4	
		3	3.0	2.4	3.0	27.9	27.8	30.4	24.8	24.3	27.4	
	100	2	3.0	2.4	3.0	30.4	29.1	34.6	26.7	25.7	31.0	
		3	3.0	2.2	3.0	33.7	32.4	38.2	29.8	28.9	33.9	
	500	2	5.2	4.7	5.6	37.2	35.2	47.6	34.0	31.2	42.6	
		3	5.2	4.8	5.8	42.0	39.0	55.0	38.9	35.1	49.1	

(2011); [Filippone et al. \(2013\)](#)). Chromatic sampling is implemented for individual locations. We used the package `GpGp` ([Joseph Guinness \(2018\)](#)) for Vecchia factor computation. Our implementation allows to run several chains in parallel thanks to the package `parallel` ([R Core Team \(2018b\)](#)), but `GpGp` does not allow parallel Vecchia factor computation within each chain like `spNNGP`. We emphasized the ease of use, with real-time Gelman-Rubin diagnostics and chains plotting, greedy MCMC tuning in the first hundred iterations, and the possibility to start, stop, and run again easily. For some data sets, our implementation has an advantage over `spNNGP` because multiple measurements at the same spatial site are allowed. However, unlike `spNNGP`, we have only implemented a Gaussian model so far.

## 4.2 Toy examples

We present two toy examples in order to test our implementation, with the latent field NNGP implementation of `spNNGP` as a reference. For both implementations, 5 nearest neighbors were used for NNGP. The toy examples are Gaussian. We compare the MCMC behavior using the number of iterations and the time needed before the chains have mixed following the Gelman-Rubin-Brooks  $\hat{R}$  ([Gelman and Rubin \(1992\)](#); [Brooks and Gelman \(1998\)](#)). We also compare the estimated covariance parameters with the values that were used to simulate the toy example. The covariance parameters are reported individually, and in the second toy example we report the Mean Square Error (MSE) of the fitted fixed effects with respect to their true value. Eventually we compare the quality of the denoising using the MSE of the denoised field predicted by the model with respect to the simulated latent field. The first toy example is a simple Gaussian field simulated as follows.

1. Simulate Spatial locations  $\mathcal{S} \sim \mathcal{U}([0, 50] \times [0, 50])$
2. Simulate Latent field  $w(\mathcal{S}) \sim \mathcal{N}(0, \Sigma(\mathcal{S}))$ ,  $\Sigma(\mathcal{S})_{i,j} = \exp(-0.5\|s_i, s_j\|)$
3. Simulate Observed variable  $z(\mathcal{S}) = w(\mathcal{S}) + \epsilon(\mathcal{S})$ ,  $\epsilon(\mathcal{S}) \sim \mathcal{N}(0, 5I_n)$

The second toy example has some regressors that are highly correlated with the latent field in order to highlight the positive effect of interweaving.

1. Simulate Spatial locations  $\mathcal{S} = [\mathcal{S}_1 | \mathcal{S}_2]$ ,  $\mathcal{S}_1 \sim \mathcal{U}([0, 50])$ ,  $\mathcal{S}_2 \sim \mathcal{U}(\{0, 1, \dots, 49\})$
2. Simulate Latent field  $w(\mathcal{S}) \sim \mathcal{N}(0, \Sigma(\mathcal{S}))$ ,  $\Sigma(\mathcal{S})_{i,j} = \exp(-0.5\|s_i, s_j\|)$
3. Extract regressors from locations  $X = [\mathbb{1}_{\mathcal{S}_2=1} | \mathbb{1}_{\mathcal{S}_2=2} | \dots | \mathbb{1}_{\mathcal{S}_2=49}]$

4. Simulate regression coefficients  $\beta \sim \mathcal{N}(0, I_{49})$
5. Simulate Observed variable  $z(\mathcal{S}) = w(\mathcal{S}) + X\beta^T + \epsilon(\mathcal{S})$ ,  $\epsilon(\mathcal{S}) \sim \mathcal{N}(0, 5I_n)$

The results of the runs on the toy examples are presented in table 6. The estimates are close to the target and there is no clear gap between the methods.

Due to the fast-mixing ASIS architecture ([Yu and Meng \(2011\)](#)), our implementation needed much less iterations than `spNNGP` (Even taking into account the fact that one ASIS iteration needs two covariance parameters updates) : 4000 iterations in the first toy example and 2400 in the second, against 15000 and 25000. The running times end up being of the same order : 47 minutes for our implementation and 28 minutes for `spNNGP` on the first toy example, and 29 minutes for our implementation against 61 for `spNNGP` in the second.

Let's now focus on the behavior of the regression coefficients in the second toy example (Figure 5). For our implementation, the  $\hat{R}$  diagnostics dropped to 1 in a few hundred iterations (figure 5a), against the tenths of thousands needed for `spNNGP` (figure 5b). The autocorrelations dropped to 0 after 50 iterations for our implementation (figure 5e). With a lag of 100, `spNNGP`'s autocorrelations were still between 0.6 and 0.8 (figure 5d). It is then clear that the chains behave much better in our implementation than in `spNNGP`. This behavior could not be reproduced by our implementation if we did not precise that interweaving could be used, see figures 5c, 5f. Therefore, we can be sure that it is our centering that caused the better behavior of the regression coefficients.

## 4.3 Application on a real data set

We used our implementation to study a heavy metal contamination data set proposed by [Hengl \(2009\)](#)<sup>1</sup>. The dataset gathers measurements made by the United States Geological Survey ([Grossman et al. \(2004\)](#)) and several covariates, including geophysical and environmental information about the sampling site, and potential contamination sources nearby. We added the predominant subsoil rock type given by the USGS study ([Horton \(2017\)](#))<sup>2</sup>. We scaled the quantitative regressors. After removing missing data, there was 64274 observations. We assumed the model

$$\log(z(s)) = w(s) + X(s)\beta^T + \epsilon(s) \quad ,$$

$s$  being the sampling location,  $X(\cdot)$  being the aforementioned covariates,  $w(\cdot)$  being a latent Gaussian field

<sup>1</sup> <https://spatial-analyst.net/book/NGS8HMC>

<sup>2</sup> <https://mrddata.usgs.gov/geology/state/>

Table 6: Summary of the toy examples runs

(a) Summary of the first toy example							
method	n iter.	time (min)	MSE	latent var.	noise var.	latent range	
spNNGP	15000	28	0.40	1.07	4.99	1.10	
Our code	4000	47	0.38	1.09	5.00	0.99	
true values			1.00	5.00	1.00		

(b) Summary of the second toy example								
method	n iter.	time (min)	MSE	$\beta$ -MSE	latent var.	noise var.	latent range	
spNNGP	25000	61	0.42	0.06	1.00	5.05	0.99	
Our code	2400	29	0.41	0.07	0.98	5.10	1.09	
true values					1.00	5.00	1.00	

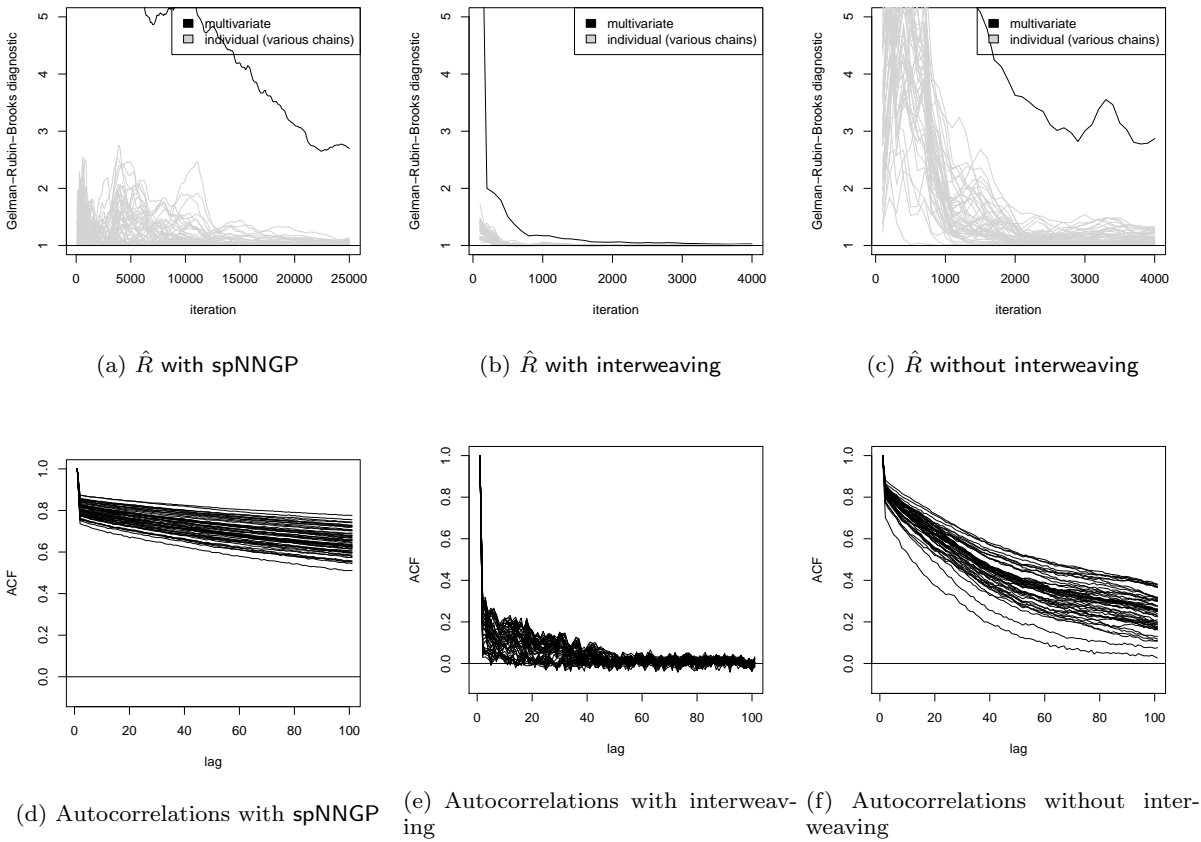


Fig. 5: Behavior of the regression coefficients with spNNGP and with our implementation

with exponential covariance on the sphere, and  $\epsilon$  being a white noise.

The model converged in 2400 iterations, and 1 hour and 3 minutes were needed. We present estimates of the covariance parameters and some of the fixed effects in table 7. We left out some regressors such as the geological classification, indications about nearby mineral observations, the geophysical characteristics of the sampling site. The variances of the latent field and the noise have equivalent order ( $\sigma^2 = 0.20, \tau^2 = 0.18$ ). The spa-

tial effect range is 30 Km. With a rule of the thumb, this means that the correlation drops to 10% of the scale for locations separated by 60 Km. The regressors behave as expected : the urbanization level and contamination indicators have a positive, certain effect on lead concentration. However, the value of the regression coefficients remains modest with respect to the scale of the latent field.

We also provide prediction of the latent field on a 5-Km grid on the territory of the USA mainland. Predictions

at un-observed locations are done using the MCMC samples of the covariance parameters  $\theta$  and  $w(\mathcal{S})$ , see for example [Finley et al. \(2019\)](#).

We report the predicted latent mean and standard deviation in figures [6a](#) and [6b](#). The standard deviation map must be put in relation with the sampling sites map (Figure [7](#)). The patches with high standard deviation correspond to zones with no measurement, while territories with dense sampling, such as Florida, will have low predicted standard deviation.

## 5 Discussion

We presented two ways to improve the behavior of NNGP with full data augmentation, that can be simply applied to previous implementations. What's more, while we assumed a Gaussian data model throughout the article, the two methods we proposed can be easily applied to other models.

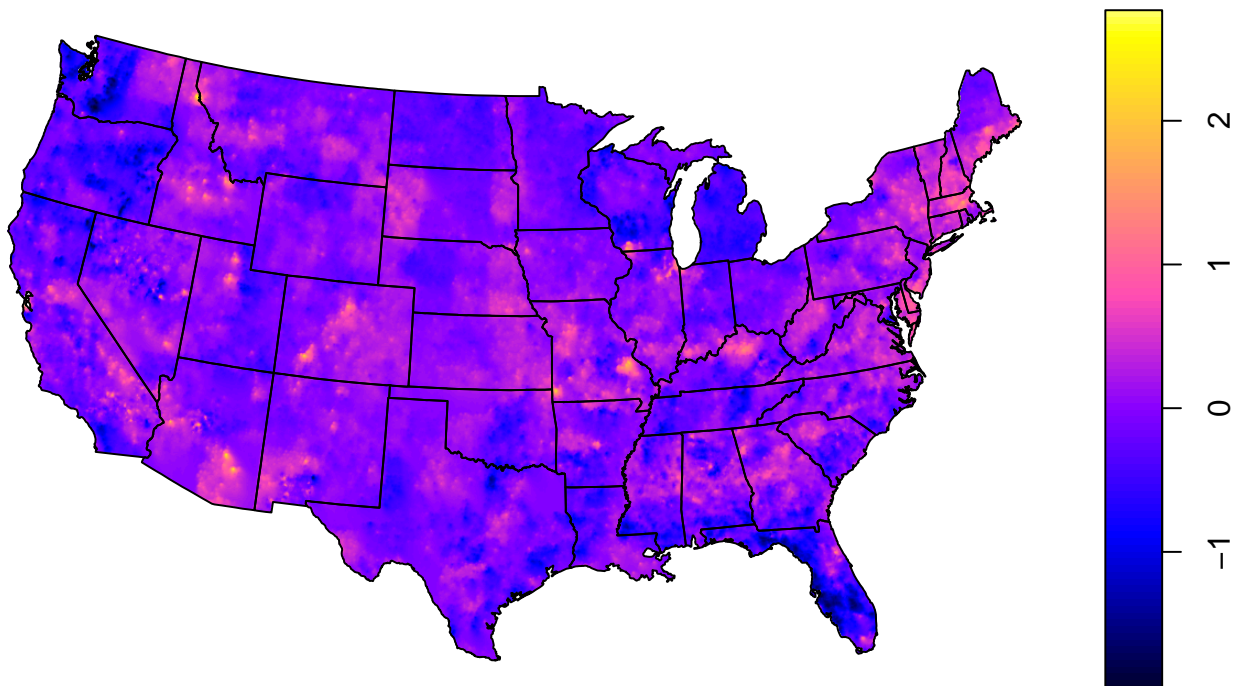
While our article focused on a basic NNGP model, our field centering may have applications in complex models. Space-varying regression coefficients are an extension to Gaussian Process models ([Datta et al. \(2016\)](#); [Banerjee et al. \(2008\)](#)). If we consider the latent field  $w(\cdot)$  as a space-varying intercept, it seems natural to try to center a spatially variable parameter on the corresponding fixed effect. The extension to other fixed effects we presented could prove valuable in the case in which the regressor with a spatially variable  $\beta$  is correlated with other variables from  $X$ . Another possible extension could be a Gaussian Process defined as the sum of two or more Gaussian Processes. It could have an interest in various applications, such as : modelling seasonality in a space-time process, modelling a process with short-range and long-range interactions, defining one non-separable space-time process as a sum of two separable processes. The equivalent of standard parametrization would be  $z(\cdot) = \beta_0 + w_1(\cdot) + w_2(\cdot) + \epsilon$ ,  $w_1(\cdot)$  and  $w_2(\cdot)$  being Gaussian Processes of mean 0. One could try out a Russian doll centering :  $z(\cdot) = v_1(\cdot) + \epsilon$  where  $v_1(\cdot)$  has mean  $v_2(\cdot)$ , and  $v_2(\cdot)$  has mean  $\beta_0$ . In this case, in addition to apply the extension to other fixed effects we presented, it might be necessary to interweave the standard and the "russian doll" parametrizations.

Beyond the improvements of chromatic sampling in the NNGP algorithm, exploration of the moralized graph could be an interesting approach to study Vecchia's approximation and evaluate heuristics concerning ordering and picking parents. For example, [Guinness \(2018\)](#) has explored how various ordering and grouping strategies affected the Kullback-Leibler divergence of Vec-

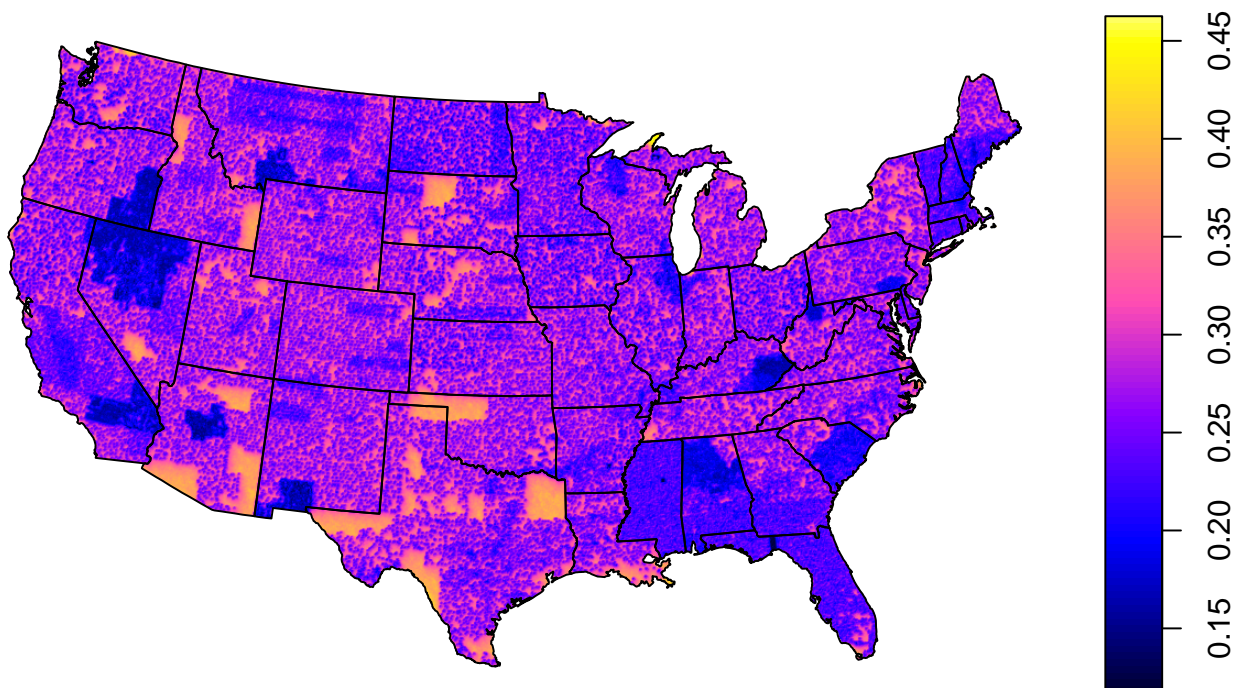
chia's approximation with respect to the full Gaussian Process density. Those strategies have a graphical translation. Grouping takes an existing graph and adds new edges, making it closer to the full GP's graph (i.e. the saturated DAG and moralized graph). Ordering modifies the structure of the graph and the length of the edges, just like the mixing of observations explored in [Stein et al. \(2004\)](#). For example, a coordinate or a middle-out ordering with Nearest Neighbor heuristic will make graph where each vertex connected to its closest neighbors, while we could use a classical concept of Geography and say that a random or a max-min ordering will generate graphs not unlike a Christallerian system. Focusing on the neighbor-picking heuristics allows to have a close-up shot of what is going on and has a direct algorithmic translation, but some descriptive statistics about the moralized graphs could give a more general view.

## References

- Banerjee S, Gelfand AE, Finley AO, Sang H (2008) Gaussian predictive process models for large spatial data sets. *Journal of the Royal Statistical Society: Series B (Statistical Methodology)* 70(4):825–848, DOI 10.1111/j.1467-9868.2008.00663.x, URL <http://doi.wiley.com/10.1111/j.1467-9868.2008.00663.x> [12](#)
- Brooks SP, Gelman A (1998) General methods for monitoring convergence of iterative simulations. *Journal of computational and graphical statistics* 7(4):434–455 [8](#), [10](#)
- Datta A, Banerjee S, Finley AO, Gelfand AE (2016) Hierarchical nearest-neighbor gaussian process models for large geostatistical datasets. *Journal of the American Statistical Association* 111(514):800–812 [2](#), [3](#), [5](#), [6](#), [7](#), [8](#), [12](#)
- Eddelbuettel D, François R, Allaire J, Ushey K, Kou Q, Russel N, Chambers J, Bates D (2011) Rcpp: Seamless r and c++ integration. *Journal of Statistical Software* 40(8):1–18 [8](#)
- Filippone M, Zhong M, Girolami M (2013) A comparative evaluation of stochastic-based inference methods for gaussian process models. *Machine Learning* 93(1):93–114 [10](#)
- Finley A, Datta A, Banerjee S (2017) spnngp: spatial regression models for large datasets using nearest neighbor gaussian processes. R package version 01 [1](#) [2](#), [3](#), [8](#)
- Finley AO, Datta A, Cook BD, Morton DC, Andersen HE, Banerjee S (2019) Efficient algorithms for bayesian nearest neighbor gaussian processes.



(a) Predicted latent mean



(b) Predicted latent standard deviation (closely related to sampling density)

Fig. 6: Latent field predictions



Table 7: Summary of the covariance parameters and a subset of the fixed effects

	mean	quantile 0.025	median	quantile 0.975	standard deviation
Scale	0.199	0.189	0.198	0.210	0.00522
Noise variance	0.178	0.175	0.178	0.181	0.00164
Range (Km)	35.8	33.5	35.7	38.6	1.25
(Intercept)	2.83	2.80	2.83	2.87	0.0195
Air pollution density	0.0400	0.0192	0.0400	0.0613	0.0107
Mineral operations density	0.0182	0.00514	0.0183	0.0306	0.00651
Industrial toxic reject density	0.0637	0.0428	0.0641	0.0833	0.0103
Carbon biomass density	-0.0539	-0.0661	-0.0538	-0.0414	0.00639
Population density	0.135	0.110	0.135	0.159	0.0125
Night light	0.0386	0.0304	0.0386	0.0467	0.00413
Roads density	0.0193	0.0138	0.0193	0.0248	0.00276

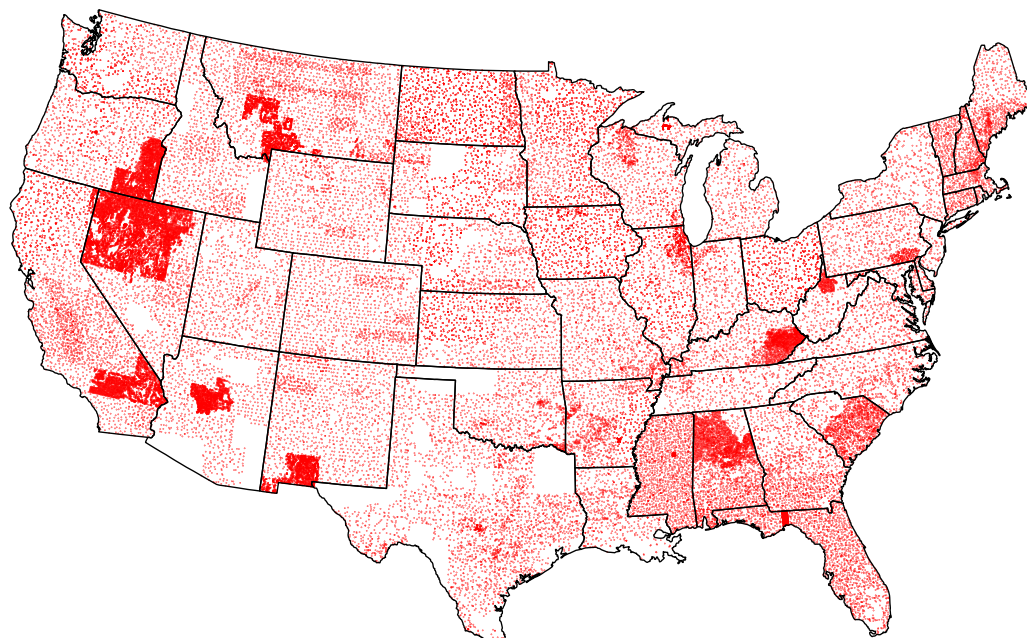


Fig. 7: Sampling sites

Journal of Computational and Graphical Statistics  
28(2):401–414 [2](#), [3](#), [12](#)  
Fuglstad GA, Simpson D, Lindgren F, Rue H (2015)  
Interpretable priors for hyperparameters for gaussian  
random fields. arXiv preprint arXiv:150300256 [2](#)  
Gelfand AE, Sahu SK, Carlin BP (1995) Efficient  
parametrisations for normal linear mixed models.  
Biometrika 82(3):479–488 [3](#)

Gelfand AE, Diggle P, Guttorp P, Fuentes M  
(2010) Handbook of Spatial Statistics (Chapman  
& Hall CRC Handbooks of Modern Statistical  
Methods). Chapman & Hall CRC Handbooks of  
Modern Statistical Methods, Taylor and Fran-  
cis, URL [http://gen.lib.rus.ec/book/index.  
php?md5=96CFC718B8554AB6448050DB14685E28](http://gen.lib.rus.ec/book/index.php?md5=96CFC718B8554AB6448050DB14685E28) [1](#)  
Gelman A, Rubin DB (1992) Inference from iterative  
simulation using multiple sequences. Statistical sci-

- ence 7(4):457–472 [8](#), [10](#)
- Gonzalez JE, Low Y, Gretton A, Guestrin C (2011) Parallel gibbs sampling: From colored fields to thin junction trees [3](#), [5](#)
- Grossman JN, et al. (2004) The National Geochemical Survey-database and documentation [10](#)
- Guinness J (2018) Permutation and grouping methods for sharpening gaussian process approximations. *Technometrics* 60(4):415–429, DOI 10.1080/00401706.2018.1437476, URL <https://doi.org/10.1080/00401706.2018.1437476>, <https://doi.org/10.1080/00401706.2018.1437476> [2](#), [6](#), [12](#)
- Heinonen M, Mannerström H, Rousu J, Kaski S, Lähdesmäki H (2016) Non-stationary gaussian process regression with hamiltonian monte carlo. In: *Artificial Intelligence and Statistics*, pp 732–740 [2](#)
- Hengl T (2009) *A practical guide to geostatistical mapping*. Hengl Amsterdam [10](#)
- Horton JD (2017) The state geologic map compilation (sgmc) geodatabase of the conterminous united states [10](#)
- Joseph Guinness M (2018) GpGp: Fast Gaussian Process Computation Using Vecchia’s Approximation. URL <https://CRAN.R-project.org/package=GpGp> [2](#), [10](#)
- Katzfuss M, Guinness J (2017) A general framework for Vecchia approximations of Gaussian processes. arXiv e-prints arXiv:1708.06302, [1708.06302](#) [2](#), [5](#)
- Knorr-Held L, Rue H (2002) On block updating in markov random field models for disease mapping. *Scandinavian Journal of Statistics* 29(4):597–614 [2](#), [5](#), [7](#)
- Lauritzen SL (1996) *Graphical models*. Oxford Statistical Science Series, OUP, URL <http://gen.lib.rus.ec/book/index.php?md5=7ECA79CDE5FF909E7E0E7FC8A02D8A80> [5](#)
- R Core Team (2018a) *R: A Language and Environment for Statistical Computing*. R Foundation for Statistical Computing, Vienna, Austria, URL <https://www.R-project.org/> [8](#)
- R Core Team (2018b) *R: A Language and Environment for Statistical Computing*. R Foundation for Statistical Computing, Vienna, Austria, URL <https://www.R-project.org/> [10](#)
- Rue H, Held L (2005) *Gaussian Markov random fields: theory and applications*, 1st edn. Monographs on statistics and applied probability 104, Chapman & Hall/CRC, URL <http://gen.lib.rus.ec/book/index.php?md5=800474D84710FBE4C4F989801371938A> [2](#)
- Stein ML (1999) *Interpolation of Spatial Data: Some Theory for Kriging*, 1st edn. Springer Series in Statistics, Springer-Verlag New York, URL <http://gen.lib.rus.ec/book/index.php?md5=e2da912dee4e6b700d99ddb258ef8d4a> [2](#)
- Stein ML, Chi Z, Welty LJ (2004) Approximating likelihoods for large spatial data sets. *Journal of the Royal Statistical Society: Series B (Statistical Methodology)* 66(2):275–296 [2](#), [12](#)
- Yu Y, Meng XL (2011) To center or not to center: That is not the question—an ancillarity–sufficiency interweaving strategy (asis) for boosting mcmc efficiency. *Journal of Computational and Graphical Statistics* 20(3):531–570 [2](#), [3](#), [8](#), [10](#)